光学学报

基于非线性频率变换的长波红外激光器研究进展

白振旭[1,2*]，高嘉[1,2]，赵臣[1,2,3]，颜秉政[1,2]，齐瑶瑶[1,2]，丁洁[1,2]，王雨雷[1,2]，吕志伟[1,2**]

[1]河北工业大学先进激光技术研究中心，天津 300401；

[2]河北省先进激光技术与装备重点实验室，天津 300401；

[3]光电信息控制和安全技术重点实验室，天津 300308

摘要　8～12 μm长波红外波段激光位于大气传输窗口并覆盖诸多气体分子的吸收带，在大气探测、光电对抗等领域具有重要的应用。目前，通过粒子数反转激光器直接辐射以及非线性频率变换间接辐射是实现8～12 μm长波红外激光输出的主要方式。其中，基于非线性光学晶体频率转换的长波红外激光器具有结构紧凑、波长选择灵活、功率拓展性强等优势，近年来得到了快速发展和广泛应用。本文对二阶非线性频率变换的光学晶体、工作原理，以及获得长波红外激光的研究进展进行综述，并对基于受激拉曼散射的三阶非线性频率变换获得长波红外的方法进行了介绍和展望。

关键词　激光器；长波红外激光；非线性频率变换；8～12 μm；非线性晶体

中图分类号　TN248.1　　**文献标志码**　A　　**DOI**：10.3788/AOS221126

1　引　　言

8～12 μm长波红外激光位于大气传输窗口和人眼安全范围，在大气介质中传输具有更高的透过率，因此在定向红外对抗[1-2]、环境监测[3-4]和激光雷达[5-6]等领域具有重要应用，同时也被广泛应用于外科手术等激光医疗领域[7-8]。红外激光大气透射光谱及主要吸收粒子如图1所示。具体来说，8～12 μm长波红外波段包含了H_2O、CO_2、NH_3及O_3等气体分子和有毒气体的基频吸收带，因此该波段激光在环境监测和差分吸收雷达方面有着重要作用[9]；在激光医疗方面，水和生物组织中的其他成分对8～12 μm长波红外激光的吸收系数大、穿透深度浅，使得长波红外激光在生物组织治疗领域成为独特而有效的方法；同时，高能量、高光束质量的8～12 μm长波红外激光器在国防和军事方面的需求也十分迫切。

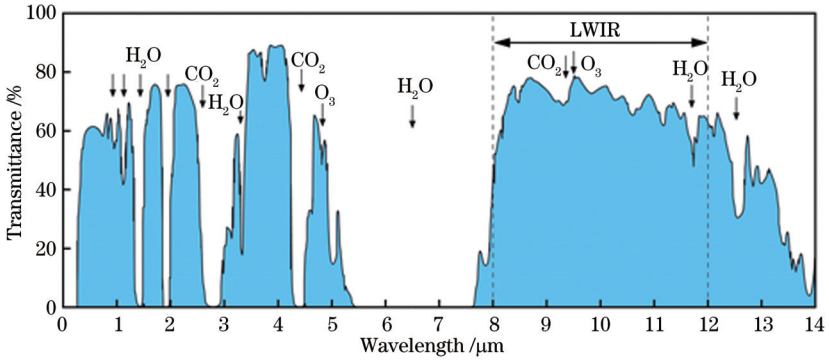

图1　红外激光大气透射光谱及主要吸收粒子

Fig. 1　Infrared laser atmospheric transmission spectrum and main absorbing particles

目前获得8～12 μm长波红外激光的方法主要包括以二氧化碳(CO_2)激光器和半导体量子级联激光器(QCL)为代表的增益介质“直接辐射”，以及以二阶非线性频率变换(非线性光学技术)为代表的“间接辐射”，图2展示了3种方法的发展历程。世界上第一台二氧化碳激光器由贝尔实验室的Patel[10]于1964年发

收稿日期：2022-05-13；**修回日期**：2022-07-14；**录用日期**：2022-08-12；**网络首发日期**：2022-08-20

基金项目：国家自然科学基金重大科研仪器研制项目(61927815)、中国科学院功能晶体与激光技术重点实验室开放课题(FCLT202004)、量子光学与光量子器件国家重点实验室开放课题(KF202201)、河北工业大学基本科研业务费资助(JB-KYTD2201)。

通信作者：*baizhenxu@hotmail.com；**zhiweilv@hebut.edu.cn

明，它是一种以气体混合物为增益介质的激光器。现阶段，二氧化碳激光器是8～14 μm波段成熟的相干辐射源，其发展较早、商业产品较为成熟，主要应用和发展方向包括波导二氧化碳激光器、横向激励大气压二氧化碳激光器等[11-12]。二氧化碳激光器具有输出功率高、脉冲能量大等突出优势，但输出波长局限于9.2～9.8 μm及10.1～11 μm范围内，无法覆盖整个长波红外波段，且调谐性能不佳；此外，由于二氧化碳激光器的泵浦利用率较低，有大量能量转化为热能，因此通常需要配套大型的冷却系统，这导致装置体积庞大，很大程度上限制了其应用范围[13-14]。量子级联激光器是基于半导体耦合量子阱子带间电子跃迁的一种单极性光源，作为一种新型的半导体激光器，其输出波长能够覆盖长波红外波段[15]。第一台量子级联激光器在1994年诞生于贝尔实验室，由Faist等[16]首次制成，随后人们又陆续实现了分布反馈式量子级联激光器[17]、室温下连续工作的量子级联激光器[18]等。量子级联激光器具有非常宽的发射光谱（3.5～160 μm），且具有半导体激光器显著的可集成和轻型化的特征。但是，量子级联激光器的量子阱深度有限，导致其在8～12 μm波段效率较低，且设计难度大，难以实现高功率高脉冲能量的运转[19-21]。

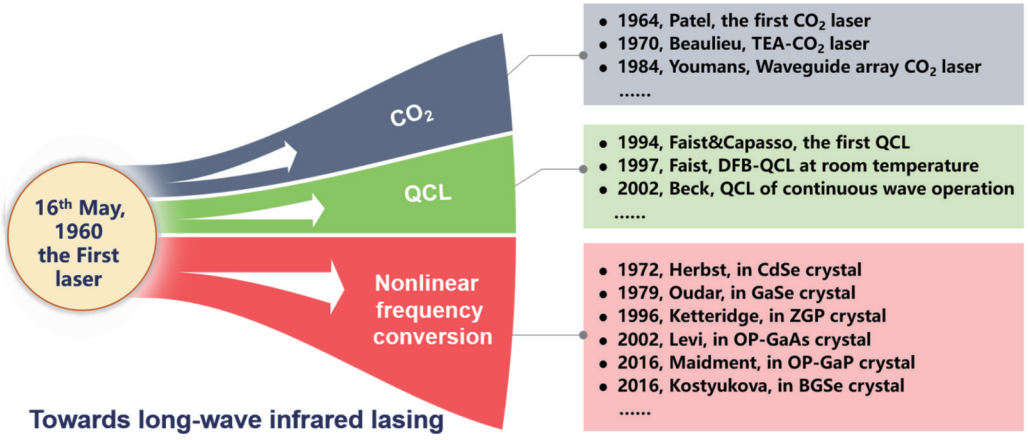

图2　二阶非线性频率变换、二氧化碳激光器与量子级联激光器的发展状况[10-12,16-18,22-27]

Fig. 2　Development of second-order nonlinear frequency conversion, CO_2 lasers, and QCL[10-12,16-18,22-27]

虽然以气体和半导体为增益介质已经实现了8～12 μm长波红外激光输出，但是通过直接泵浦晶体增益介质获得长波红外激光直接辐射尚无成熟方法[28-29]，以二阶非线性频率变换技术为“桥梁”是目前产生8～12 μm长波红外激光输出最成熟也是最广泛使用的手段。二阶非线性频率变换技术是利用光学介质在强辐射场下的二阶非线性光学效应产生新的频率，包括光参量产生（OPG）、光参量振荡（OPO）、差频（DFG）和光参量放大（OPA）等。目前，人们已经利用磷锗锌（$ZnGeP_2$，ZGP）、硒化镉（CdSe）、硒化镓（GaSe）、硒镓钡（$BaGa_4Se_7$，BGSe）、硫镓锂（$LiGaS_2$，LGS）、取向图案化砷化镓（OP-GaAs）、取向图案化磷化镓（OP-GaP）等非线性晶体[22-27]通过二阶非线性频率变换实现8～12 μm长波红外激光输出。值得一提的是，基于二阶非线性频率变换技术的固体激光器突破了现阶段晶体增益介质无法直接产生长波红外激光的困境。相比于二氧化碳激光器和量子级联激光器，固体激光器具有全固态化、波长可调谐的特点，并可利用各种红外非线性晶体的物理和光学特性，使激光器朝超短脉冲宽度、高重复频率、宽调谐范围和高能量等方向发展。

本文对二阶非线性频率变换技术的工作原理、常用红外非线性晶体的物理和非线性光学特性、长波红外激光器的研究进展和输出特性进行了综述，同时对基于二阶和三阶非线性频率变换技术的长波红外激光器进行了总结与展望，期待能够为从事长波红外激光器研发工作的工程技术人员提供参考。

2　用于长波红外的非线性光学晶体

二阶非线性频率变换技术的特点在于，能够直接利用成熟的1～2 μm近红外激光作为泵浦源，将其转换到8～12 μm长波红外波段。目前OPG、OPO、DFG、OPA等二阶非线性频率变换技术是获取8～12 μm长波红外激光的重要技术手段。OPG的转换过程如图3（a）所示，其过程是将一束频率为ω_3的泵浦光入射到非线性晶体中，转化为两束频率较低的参量光ω_1和ω_2，输出的光波长由相位匹配条件确定；OPO是在OPG的基础上加入谐振腔，由于谐振腔的作用，参量光往返多次通过非线性晶体从而持续放大形成参量振荡，其过程如图3（b）所示；DFG是将一束频率为ω_3的泵浦光和另一束低频率的信号光ω_1入射到非线性晶体中，两束光强度相近，通过相互作用产生一束频率更低的闲频光ω_2，其转换过程如图3（c）所示；OPA与DFG的物理过程相似，不同之处在于OPA由单个强泵浦光ω_3激发，然后对弱信号光ω_1进行放大，其转换过程如图3（d）所示。

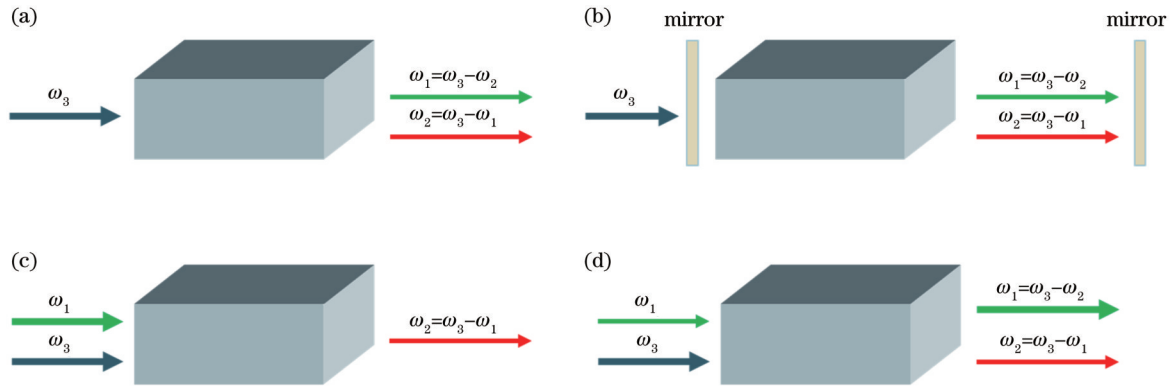

图 3　典型的二阶非线性频率变换过程示意图。(a) OPG;(b) OPO;(c) DFG;(d) OPA

Fig. 3　Schematic of typical second-order nonlinear frequency conversion processes. (a) OPG; (b) OPO; (c) DFG; (d) OPA

非线性晶体的特性是决定长波红外激光器性能的关键因素，其主要包括晶体非线性系数、透光范围、热导率以及损伤阈值等。非线性系数是激光器阈值和转换效率的关键影响因素，透光范围决定了晶体可利用的泵浦光以及输出光的波长范围，热导率的大小关系到激光器受热效应影响的程度，而损伤阈值则决定了激光器能承受的输出能量或功率的上限。表 1 所示为目前用于实现长波红外激光输出的非线性晶体的光学特性，其中 ZGP、CdSe、GaSe 等晶体发展时间长、研究较为成熟，BGSe、LGS、OP-GaAs、OP-GaP 等晶体是近年来应用于长波红外频率变换的新型非线性晶体[30]。BGSe 由中国科学院理化技术研究所于 2010 年首次成功制备[31]，LGS 晶体是用 Li 离子替换传统红外非线性晶体硫镓银($AgGaS_2$)中 Ag 离子得到的，OP-GaAs、OP-GaP 晶体是特性较为优异的准相位匹配材料[32-33]。

表 1　红外非线性晶体的光学特性

Table 1　Optical properties of infrared nonlinear crystals

Crystal	Nonlinear coefficient /(pm·V^{-1})	Transparency range /μm	Thermal conductivity /(W·m^{-1}·K^{-1})	Damage threshold /(MW·cm^{-2})
$ZnGeP_2$[34-36]	d_{14}=75	0.7-12	35	30
$BaGa_4Se_7$[37-38]	d_{11}=24.3, d_{13}=20.4	0.4-18	0.74(along a), 0.64(along b), 0.56 (along c)	557
CdSe[39-41]	d_{31}=18	0.75-25	6.9	56
GaSe[42-44]	d_{22}=56	0.6-20	16.2	30
$LiGaS_2$[45]	d_{31}=5.8	0.32-11.6	8	>240
OP-GaAs[46-47]	d_{14}=94	0.85-19	55	38
OP-GaP[47-49]	d_{14}=70.6	0.57-12	110	104

3　长波红外激光器研究进展

3.1　ZGP 长波红外激光器研究进展

ZGP 晶体的透光范围为 0.7～12 μm，其在 2 μm 处吸收系数非常低(<0.05 cm^{-1})，但是在 1 μm 处的吸收系数较高(≈1 cm^{-1})[35]。因此在实际应用中，基于 ZGP 晶体的长波红外激光器的泵浦波长通常要大于 2 μm，如采用 2.09 μm 的 Ho:YAG 激光器、2.05 μm 的 Ho:YLF 激光器，以及 Tm,Ho:$GdVO_4$ 激光器等。与其他红外非线性晶体相比，高非线性系数(d_{14}=75 pm/V)、高热导率(35 W/m·K)和适中的损伤阈值(30 MW/cm^2)使得 ZGP 晶体能够实现较低阈值的长波激光非线性频率转换，并获得中高功率的重复频率运转。目前，基于 ZGP 晶体的长波红外激光器大多采用 OPO、OPA 结构，或两者结合的级联结构，即将 OPO 系统输出的长波闲频光作为 OPA 系统的种子光，将 OPO 系统输出的信号光作为 OPA 系统的泵浦光，从而实现长波闲频光的放大，这种结构由 Bakkland 等[50]在 2016 年首次提出。表 2 展示了基于 ZGP 的长波红外激光器近年的研究进展。

由于 ZGP 晶体的透过率在 10 μm 及以上时会出现明显下降，因此目前基于 ZGP 的长波红外激光器的输出光谱集中在 8～10 μm 范围。2020 年，Liu 等[57]报道了 9.8 μm 高功率长波红外 ZGP-OPO 结构，泵浦源采用最高平均输出功率为 90 W、波长为 2.09 μm、重复频率为 10 kHz 的 Ho:YAG 主振荡功率放大器(MOPA)，利用 ZGP 晶体在基于Ⅰ类相位匹配的条件下输出最高平均功率为 3.5 W、脉冲宽度为 19.6 ns、中心波长为 9.8 μm 的长波激光，转换效率为 3.9%；在基于Ⅱ类相位配的条件下实现 9.2～11 μm 可调谐的

表 2　ZGP 长波红外激光器研究进展

Table 2　Research progress of ZGP long-wave infrared lasers

Year	λ_{pump} /μm	Output wavelength /μm	Repetition rate / kHz	Pulse duration /ns	Average power /W	Structure	Ref.
2015	2.09	8	1	28	—	OPO	[51]
2016	2.09	8.1	21	36	5.04	OPO	[52]
2016	2.09	8.3	20	34	8.2	OPO	[53]
2017	2.05	7.8-9.9[a]	10	19.5	1.71	OPO	[54]
2018	2.1	8.3	20	30.4	11.4	OPA	[55]
2019	2.09	8.2	10	21.5	12.6	OPO/OPA	[56]
2020	2.09	9.2-11[a]	10	19.6	3.5@9.8 μm	OPO	[57]
2021	2.05	8.1	10	27.1	3.2	OPO	[58]
2021	2.1	8.2	1	8.1	3.15	OPO	[59]
2021	2.1	8.2	3	<10	5.48	OPO	[60]

Notes: [a]—wavelength tunable.

长波红外激光输出。2021 年，Qian 等[59]使用最高平均功率为 52 W、重复频率为 1 kHz、波长为 2.1 μm 的 Ho∶YAG-MOPA 系统作为泵浦源，通过 ZGP-OPO 结构获得了最高平均输出功率为 3.15 W、脉冲宽度为 8.1 ns、中心波长为 8.2 μm 的长波红外激光输出，光束质量因子 M^2 在水平和垂直方向上分别为 1.20 和 1.28。2015 年，Yu 等[51]研究了谐振腔结构、腔长及相位匹配类型对 ZGP-OPO 系统光束质量的影响，通过对比实验发现对于 8 μm 闲频光输出，更长的 OPO 谐振腔长度、环型腔结构和Ⅰ类相位匹配都有助于提高输出光的光束质量。根据这一规律，通过实验获得的最佳光束质量因子 M^2 在水平方向和垂直方向分别为 1.22 和 1.20。2019 年，Liu 等[56]使用 OPO 与 OPA 结合的级联结构，研究了 ZGP-OPO 与 ZGP-OPA 中晶体的Ⅰ类和Ⅱ类相位匹配对级联系统输出性能的影响，实验装置如图 4 所示。该级联结构的特点在于，OPA 部分使用 OPO 输出的 2.8 μm 信号光作为泵浦光，实现对 8.2 μm 闲频光放大，因此既能够提高闲频光的输出功率，又能充分利用闲置的信号光，进而提高光-光转换效率。该实验利用最高平均输出功率为 100 W、波长为 2.09 μm、重复频率为 10 kHz 的 Ho∶YAG 激光器作为泵浦源，在基于Ⅱ类相位匹配的 ZGP-OPO 和Ⅰ类相位匹配的 ZGP-OPA 级联系统中，获得了最高平均功率为 12.6 W、脉冲宽度为 21.5 ns 的 8.2 μm 激光输出，对应的转换效率为 12.6%，这是 ZGP 长波红外激光器目前取得的最高功率。

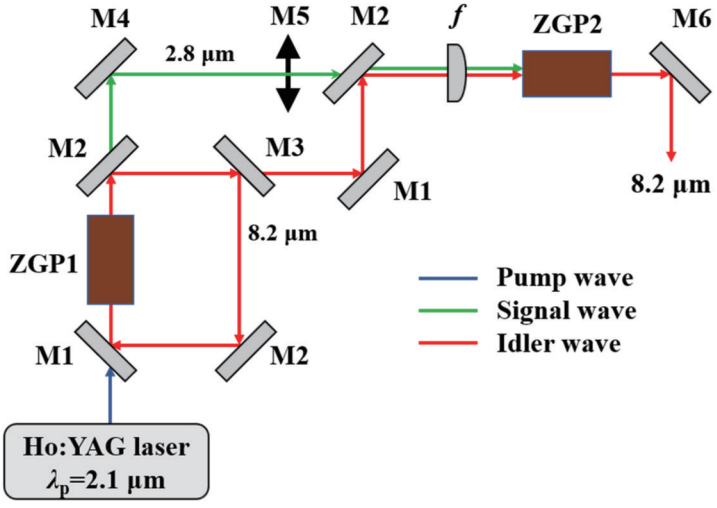

图 4　ZGP-OPO 长波红外激光器[56]

Fig. 4　ZGP-OPO long-wave infrared laser[56]

3.2　BGSe 长波红外激光器研究进展

BGSe 晶体的非线性系数 d_{11}=24.3 pm/V、d_{13}=20.4 pm/V，透光范围为 0.4～18 μm，与 ZGP 等非线性晶体不同的是，BGSe 晶体的带隙宽度为 2.73 eV，因此它可以使用成熟的 1 μm 激光器作为泵浦源。同时，BGSe 晶体的损伤阈值高达 557 MW/cm^2，因此能够承受更高的泵浦功率或更大的脉冲能量。然而，BGSe 晶体的热导率较低，沿 a、b、c 轴的热导率

分别为 0.74、0.67、0.56 W·m^{-1}·K^{-1}[37]，这导致其难以在高重复频率泵浦下实现稳定运转。表 3 展示了近年来基于 BGSe 晶体的长波红外激光器的研究进展。

表 3　BGSe 长波红外激光器的研究进展

Table 3　Research progress of BGSe long-wave infrared lasers

Year	λ_{pump} /μm	Output wavelength /μm	Repetition rate	Pulse duration	Average power or energy	Structure	Ref.
2016	1.06	2.7-17[a]	10 Hz	10 ns	<4.5 mJ	OPO	[30]
2018	2.1	8-9[a]	1 kHz	16 ns	314 mW@8.9 μm	OPO	[61]
2019	1.05	2.6-10.4[a]	100 Hz	ns level	14 μJ@8 μm	OPO	[62]
2019	2.79	3.9-9.5[a]	10 Hz	21 ns	<3.5 mJ	OPO	[63]
2020	1.06	8-14[a]	10 Hz	22.3 ps	230 μJ @9.5 μm	OPA	[64]
2020	1.06	8-14[a]	10 Hz	10.1 ns	1.05 μJ@11 μm	OPO	[65]
2020	2.4	6-18[b]	69 MHz	42 ps	<1.9 mW	IPDFG	[66]

Notes: [a]—wavelength tunable; [b]—broad spectrum.

在 1 μm 激光泵浦 BGSe 产生长波红外激光方面，2019 年，Kolker 等[62]使用波长为 1.05 μm、脉冲宽度为 16 ns、重复频率为 100 Hz 的 Nd∶YLF 激光器作为泵浦源，采用基于Ⅰ类相位匹配的线型腔 BGSe-OPO 结构，实验得到了 2.6～10.4 μm 可调谐红外激光，8 μm 处脉冲能量为 14 μJ，装置如图 5 所示。2020 年，Yang 等[64]报道了一台 8～14 μm 连续可调谐的高能量皮秒级 BGSe-OPA 长波红外激光器，BGSe 晶体为Ⅰ类相位匹配，泵浦源采用重复频率为 10 Hz、脉冲宽度为 30 ps、波长为 1064 nm 的 Nd∶YAG 激光器，种子光（信号光）在 1151～1227 nm 波长范围内连续可调谐，能量范围为 0～200 μJ，该实验最终实现脉冲能量为 140～230 μJ、波长为 8～14 μm 连续可调的长波红外激光输出，9.5 μm 处能量最高为 230 μJ，脉冲宽度约为 22.3 ps。Xu 等[65]使用脉冲能量为 39.5 mJ、波长为 1.06 μm、重复频率为 10 Hz、脉冲宽度为 10 ns 的 Nd∶YAG 激光器作为泵浦源，采用基于Ⅰ类相位匹配的 BGSe-OPO 结构，最终实现 8～14 μm 可调谐的长波红外激光输出，11 μm 处脉冲能量最高为 1.05 mJ，转换效率为 2.65%。

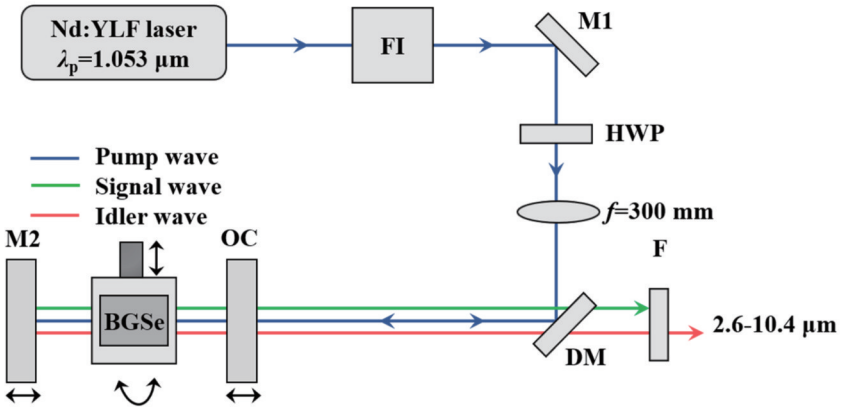

图 5　红外可调谐 BGSe-OPO 激光器[62]

Fig. 5　Infrared tunable BGSe-OPO laser[62]

除了使用 1 μm 光源泵浦外，BGSe 同样可以使用 2 μm 等更长波长的泵浦源，且理论上具有更高的频率转换效率。Hu 等[63]使用波长为 2.79 μm、由 Cr，Er∶YSGG 振荡级和放大级组成的调 Q 激光器作为泵浦源，采用基于Ⅰ类相位匹配的 BGSe-OPO 结构，最终得到 3.9～9.5 μm 的可调谐激光，其脉冲宽度为 21 ns，脉冲能量为 3.5 mJ，重复频率为 10 Hz，转换效率为 18.9%。Zhang 等[66]使用 2.4 μm 由 Cr∶ZnS 振荡级和放大级组成的激光器泵浦了 BGSe 脉冲内差频（IPDFG）结构，所用泵浦光的重复频率为 69 MHz、最高平均功率为 3.3 W，BGSe 基于Ⅰ类相位匹配，实验得到了脉冲宽度为 42 ps、6～18 μm 宽光谱的红外激光输出，平均输出功率约为 1.9 mW。

3.3　CdSe 和 GaSe 长波红外激光器研究进展

CdSe 和 GaSe 晶体被应用于二阶非线性频率变换已有数十年的历史，关于这两种晶体用于长波红外激光器的研究较为成熟。CdSe 不仅具有较低的热导率（6.9 W·m^{-1}·K^{-1}）、较小的有效非线性系数（d_{31}=18 pm/V）、适中的损伤阈值（56 MW/cm^2）等特点，而

且具有非常适用于长波红外的非线性频率变换透过光谱范围(0.75～25 μm),尤其是在1～10 μm波长范围内的吸收系数非常低(<0.05 cm^{-1}),且对大于8 μm波长范围的调谐效率无多声子吸收[39]。相比于CdSe晶体,GaSe具有更高的热导率(16.2 $W·m^{-1}·K^{-1}$)和非线性系数(d_{31}=56 pm/V),还有相当宽的透过光谱范围(0.6～20 μm)。表4展示了基于CdSe和GaSe的长波红外激光器近年的研究进展。

表4　CdSe和GaSe长波红外激光器研究进展

Table 4　Research progress of CdSe and GaSe long-wave infrared lasers

Crystal	Year	λ_{pump} /μm	Output wavelength /μm	Repetition rate	Pulse duration	Average power or energy	Structure	Ref.
CdSe	2016	2.09	10-11.1[a]	500 Hz	19 ns	140 mW@10 μm	OPO	[67]
	2017	2.09	10-12.07[a]	1.2 kHz	40 ns	170 mW@12 μm	OPO	[68]
	2018	2.05	10.2	5 kHz	ns level	320 mW	OPO	[69]
	2020	2.09	9.9-10.7[a]	1 kHz	24.4 ns	1.05 W@10.1 μm	OPO	[70]
	2020	2.09	10.55-12[a]	1 kHz	21 ns	802 mW@11 μm	OPO	[71]
	2021	2.09	10.15/11	1 kHz	ns level	1.03/1.18 W	OPO	[72]
	2021	2.05	12.5	5 kHz	24.4 ns	0.1 mJ	OPO	[73]
GaSe	2018	1.92	7.3-16.5[b]	1.25 MHz	<100 fs	450 mW	IPDFG	[74]
	2018	2	9-16[a]	10 kHz	11 ns	0.36 mW@9.6 μm	DFG	[75]
	2019	3	7-15[b]	10 kHz	65 fs	1.06 μJ	IPDFG	[76]
	2019	2.15	4.2-16[b]	1 kHz	19 fs	3.4 μJ	OPA	[77]
	2019	2	6-18[b]	50 MHz	43 fs	0.5 W	IPDFG	[78]
	2019	0.65-1.05[b]	3.7-120[b]	4 MHz	31 fs	160 pJ	IPDFG	[79]

Notes: [a]—wavelength tunable; [b]—broad spectrum.

目前,CdSe晶体仅限于实现Ⅱ类相位匹配,其长波红外激光器的输出波段主要覆盖10～12 μm[80],且可应用的频率变换技术仅限于OPO[81]。2016年,Yuan等[67]报道了一种信号光谐振CdSe-OPO结构,泵浦源采用重复频率为500 Hz、波长为2.09 μm的Ho:YAG激光器,最终实现了10～11.1 μm的可调谐红外激光输出,10.28 μm处功率为140 mW,脉冲宽度为19 ns,转换效率为2%。2017年,Yuan等[68]报道了一种输出波长为12.07 μm、最高输出功率为170 mW的CdSe-OPO结构,该结构以Ho:YAG激光器为泵浦源,实现了调谐范围为10.24～12.07 μm的激光输出,其重复频率为1.2 kHz。2020年,Yuan团队报道了一种具有连续波种子注入和腔内光束扩展功能的闲频光谐振CdSe-OPO结构[70],该谐振腔使用环形腔结构,如图6所示,输出光的调谐范围为9.9～10.7 μm,在10.1 μm处获得了1.05 W的最高平均功率,此时重复频率为1 kHz,脉冲宽度为24.4 ns,转换效率为4.69%。同年,Chen等[71]报道了一种由2.58 μm连续激光器注入的闲频光谐振CdSe-OPO结构,该激光器在11.01 μm处获得了802 mW的平均

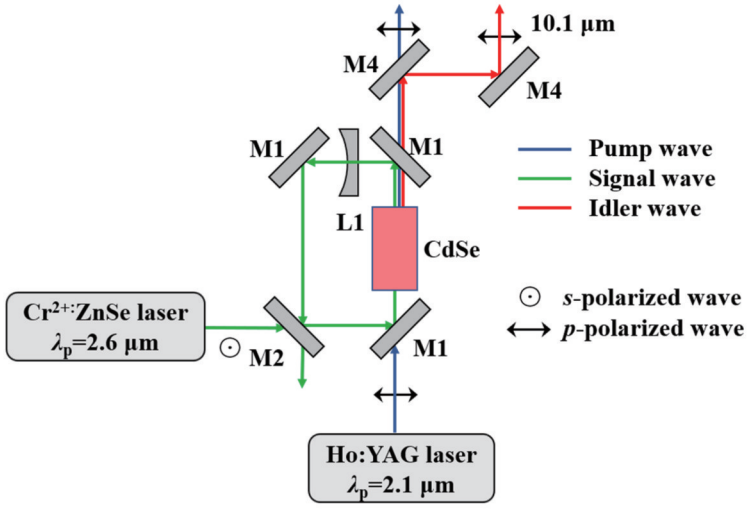

图6　可调谐CdSe-OPO长波红外激光器[70]

Fig. 6　Tunable CdSe-OPO long-wave infrared laser[70]

输出功率。2022年，Yang等[72]使用波长为2.09 μm、重复频率为1 kHz的Ho:YAG-MOPA系统作为CdSe-OPO结构的泵浦源，实验中使用两块不同尺寸的CdSe晶体，分别获得了在10.15 μm处1.03 W的最高平均输出功率和11 μm处1.18 W的最高平均输出功率。

以IPDFG和OPA技术获得高重复频率、飞秒级超短脉冲的长波红外激光是近年GaSe长波红外激光器研究的热点。2019年，Butler等[78]使用2 μm飞秒级光纤激光器作为泵浦源，采用基于Ⅰ类相位匹配的GaSe-IPDFG结构，如图7所示，获得了最高平均功率为0.5 W、重复频率为50 MHz、脉冲宽度为43 fs的6～18 μm宽光谱输出，这是目前GaSe长波红外激光器能实现的最高平均功率和重复频率。

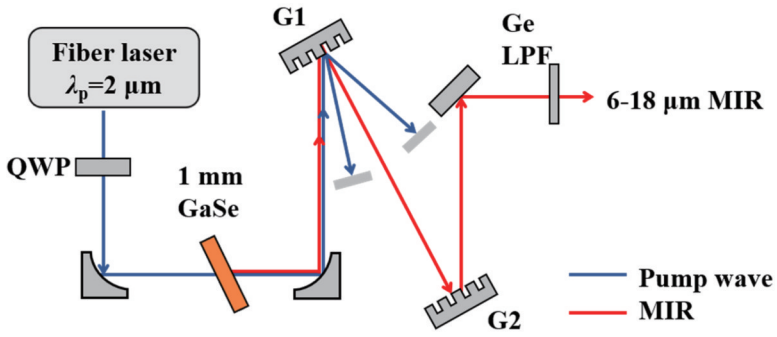

图7　高重复频率、宽光谱GaSe-IPDFG长波红外激光器[78]

Fig. 7　High repetition frequency and broad spectrum GaSe-IPDFG long-wave infrared laser[78]

3.4　LGS长波红外激光器研究进展

LGS晶体是将传统红外非线性晶体硫镓银($AgGaS_2$)中Ag离子替换为Li离子得到的。与$AgGaS_2$相比，LGS晶体具有较高的损伤阈值(>240 MW/cm^2)和较宽的透过光谱范围(0.32～11.6 μm)，但其有效非线性系数(d_{31}=5.8 pm/V)和热导率(8 W·m^{-1}·K^{-1})较低。LGS晶体的宽带隙(≈4.15 eV)使其在波长>600 nm的飞秒级脉冲激发下有着非常弱的双光子吸收[82-83]，因此LGS长波红外激光器可用钛蓝宝石(≈800 nm)或镱基(≈1030 nm)激光器作为泵浦源[84]，结合OPA、IPDFG或参量啁啾脉冲放大(OPCPA)技术，可实现长波红外波段的飞秒级脉冲输出。表5展示了基于LGS的长波红外激光器近年的研究进展。

表5　LGS长波红外激光器研究进展

Table 5　Research progress of LGS long-wave infrared lasers

Year	λ_{pump} /μm	Output wavelength /μm	Repetition rate	Pulse duration	Average power or energy	Structure	Ref.
2015	1.03	8-13[b]	100 MHz	66 fs	103 mW	IPDFG	[85]
2017	0.8	9.2-15[b]	1 kHz	73 fs	0.8 μJ	IPDFG	[86]
2018	1.03	8-11[b]	50 kHz	fs level	0.37 mW	IPDFG	[82]
2019	1.03	5-11[b]	50 kHz	32 fs	220 nJ	OPA	[87]
2019	1.03	5.7-10.5[a]	100 kHz	98 fs	< 48 mW	OPA	[88]
2019	1.03	9	10 kHz	142 fs	140 mW	OPCPA	[89]

Notes: [a]—wavelength tunable; [b]—broad spectrum.

2019年，Chen等[87]取得了目前LGS长波红外激光器的最短脉冲宽度(32 fs)，其重复频率为50 kHz、脉冲能量为220 nJ、输出波长为5～11 μm的宽光谱，实验装置采用基于Ⅰ类相位匹配的LGS-OPA结构，如图8所示，泵浦光的中心波长为1026 nm，重复频率为50 kHz，脉冲宽度为270 fs，脉冲能量为187 μJ。同年，Qu等[89]实现了目前LGS长波红外激光器的最高平均输出功率(140 mW)，其输出波长为9 μm，重复频率为10 kHz，脉冲宽度为142 fs。

3.5　OP-GaAs和OP-GaP长波红外激光器研究进展

OP-GaAs和OP-GaP是两种新型的准相位匹配晶体，通过对晶体非线性极化率进行周期性调制来实现相位匹配。OP-GaAs和OP-GaP两种晶体的制备方法为取向图案化法(orientation pattern)，即通过光刻技术制备出具有精确周期长度的反相畴模板，再以此模板为籽晶，通过氢化物气相外延方法进行厚膜生长，可以成功制备出GaAs、GaP等准相位匹配晶体[33]。该技术包括图案化衬底模板的制备和氢化物气相外延层生长两个关键过程。OP-GaAs和OP-GaP属于新型红外非线性晶体，传统长波红外非线性晶体在非线性系数、热导率、透光范围或损伤阈值的某些方面存在不足，而OP-GaAs和OP-GaP在这几个性质上几乎没有短板，

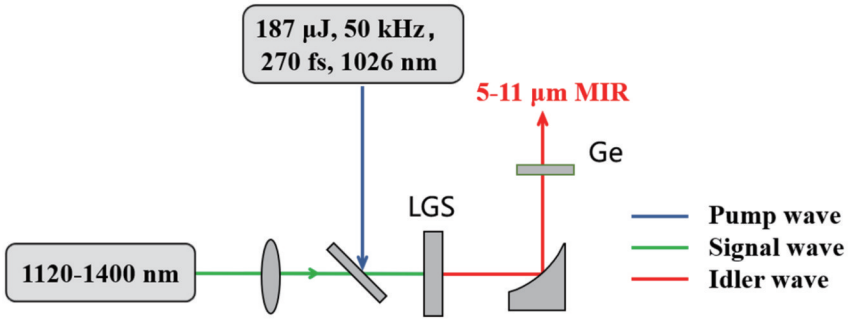

图 8　LGS-OPA 长波红外激光器[87]

Fig. 8　LGS-OPA long-wave infrared laser[87]

是性质非常优异的长波非线性晶体。OP-GaAs 拥有极高的有效非线性系数(d_{14}=94 pm/V)、较宽的透过光谱范围(0.85～19 μm)和适中的损伤阈值(38 MW/cm^2)，热导率也处于较高水平(55 W·m^{-1}·K^{-1})，但为避免双光子吸收和自由载流子吸收，OP-GaAs 通常使用波长大于 1.7 μm 的光源泵浦[90]。OP-GaP 同样拥有优异的性质，其透光范围(0.57～12 μm)和非线性系数(70.6 pm/V)与 ZGP 晶体相近，但 OP-GaP 对泵浦波长的选择更为灵活，其可用 1 μm 的光源泵浦。OP-GaP 有着很高的热导率(110 W·m^{-1}·K^{-1})和损伤阈值(104 MW/cm^2)，这表明 OP-GaP 可在高功率和高重复频率下工作。表 6 展示了基于 OP-GaAs 和 OP-GaP 的长波红外激光器近年的研究进展。

表 6　OP-GaAs 和 OP-GaP 长波红外激光器研究进展

Table 6　Research progress of OP-GaAs and OP-GaP long-wave infrared lasers

Crystal	Year	λ_{pump} /μm	Output wavelength / μm	Repetition rate	Pulse duration	Average power or energy	Structure	Period length /μm	Ref.
OP-GaAs	2014	2.99-3.15[a]	4-14[a]	2 kHz	～20 ns	＜7 μJ	OPO	150	[91]
	2015	1.94	10.3-10.9[a]	100 Hz	17 ns	2 μJ@10.3 μm	OPO	72.6	[92]
	2016	1.95	10.6	50 kHz	100 ns	812 mW	OPO	74.5	[93]
	2017	1.88-1.98[a]	8-10[a]	2 kHz	50 ns	140 W[b]@8.5 μm	OPA	66	[94]
	2018	1.05	7-9.2[a]	3 kHz	11.5 ns	＜10 mW	DFG	31.5	[95]
	2021	2.45	8.15	35 kHz	ns level	215 mW	DFG	—	[96]
OP-GaP	2016	1.04	5-12[c]	101 MHz	fs level	＜55 mW	OPO	21.5-34.0	[26]
	2018	1.04	5-13[a]	101 MHz	fs level	＜105 mW	OPO	34	[97]
	2021	1.04	3.9-12[a]	100 MHz	fs level	60 mW@10.7 μm	OPO	21	[98]

Notes: [a]—wavelength tunable; [b]—peak power; [c]—broad spectrum.

目前对于 OP-GaAs 长波红外激光器的研究，脉冲宽度主要在 ns 量级、平均功率在 mW 量级。2016 年，Wueppen 等[93]采用基于环形腔的 OP-GaAs-OPO 结构，OP-GaAs 的周期长度为 74.5 μm，在实验获得了 OP-GaAs 长波红外激光器目前最高的平均功率 812 mW，此时中心波长为 10.6 μm，重复频率为 50 kHz，脉冲宽度为 100 ns，实验所用的泵浦源波长为 1.95 μm，实验装置如图 9 所示。近年来在针对 OP-GaP 长波红外激光器的研究中，激光器的重复频率主要在百兆赫兹级，脉冲宽度在飞秒级。2021 年，Schunemann 等[98]使用 1040 nm 波长的飞秒级光纤激光器，基于 OP-GaP-OPO 结构，OP-GaP 周期长度为 21.0 μm，在实验获得了最高平均功率为 60 mW、重复频率为 100 MHz、3.9～12 μm 范围内可调谐的飞秒级红外激光输出。

3.6　小 结

近年来，基于上述非线性晶体的长波红外激光器在短脉冲宽度、高重复频率、输出波长可调谐和高功率、大脉冲能量等方面有着出色的表现。脉冲宽度方面，长波红外激光器覆盖了飞秒、皮秒、纳秒量级：GaSe、LGS、OP-GaP 长波红外激光器可实现飞秒脉冲输出；BGSe 长波红外激光器可实现皮秒脉冲输出；ZGP、BGSe、CdSe、OP-GaAs 长波红外激光器均可实现纳秒脉冲输出。重复频率方面，长波红外激光器能实现赫兹级、千赫兹级、兆赫兹级输出，LGS、OP-GaP 长波红外激光器最高可达到百兆赫兹重复频率的输出。由于非线性频率变换在长波红外波段具有量子转换效率低的特点，长波红外激光器的输出能量要低于中波红外激光器。图 10 所示为基于常见非线性晶体产生的长波红外激光器脉冲能量对比，不难发现，现阶

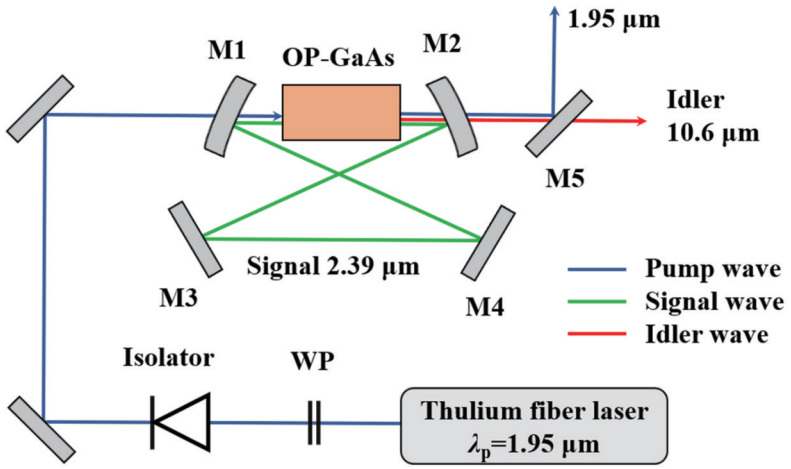

图 9　OP-GaAs-OPO 长波红外激光器[93]

Fig. 9　OP-GaAs-OPO long-wave infrared laser[93]

段长波红外激光的输出能量主要处在微焦和毫焦量级。其中：ZGP、BGSe 和 CdSe 晶体得益于自身优异的性质，基于这 3 种晶体的长波红外激光器在脉冲能量上处在较高水平，ZGP、BGSe 和 CdSe 长波红外激光器获得的最大脉冲能量分别为 3.15 mJ、4.5 mJ、1.18 mJ；基于 GaSe、LGS、OP-GaAs 晶体的长波红外激光器获得的最大脉冲能量分别为 3.4 μJ、14 μJ、16.2 μJ；OP-GaP 长波红外激光器获得的脉冲能量最小，仅能获得纳焦级的脉冲能量输出。

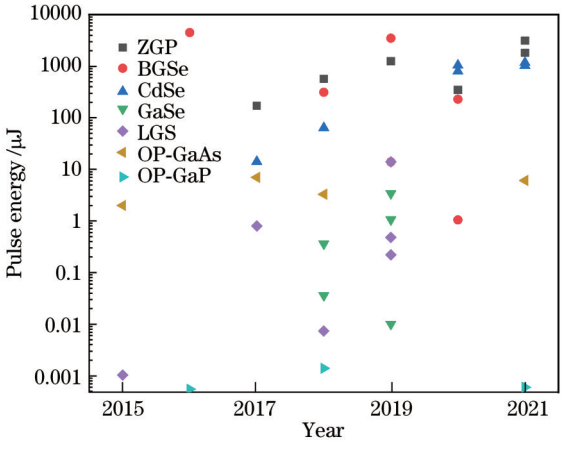

图 10　基于各类非线性晶体的长波红外激光器脉冲能量对比

Fig. 10　Comparison of pulse energy of long-wave infrared laser based on various nonlinear crystals

4　总结与展望

综述了基于二阶非线性频率变换的 ZGP、BGSe、CdSe、GaSe、LGS、OP-GaAs、OP-GaP 长波红外激光器的研究进展。目前，虽然基于二阶非线性频率变换技术的长波红外激光器取得了出色的成就，但长波红外激光器目前还无法满足所有应用场景的要求。影响二阶非线性频率变换长波激光器性能的主要因素包括非线性晶体的性质和泵浦源性能。晶体性质方面，ZGP、OP-GaP 晶体在 10 μm 后存在本征吸收峰，导致晶体吸收严重，难以获得高功率、大能量的 10～12 μm 激光输出；ZGP、GaSe、CdSe 及 OP-GaAs 晶体由于严重的双光子吸收，均需接近或大于 2 μm 的光源泵浦；LGS 和 BGSe 晶体的热导率较小，使得激光器不适合高重复频率运转。此外，目前大部分晶体无法满足长波输出所需的大尺寸晶体要求。泵浦源性能方面，1 μm 近红外激光器是目前最成熟、最可靠的泵浦源，但部分晶体无法使用 1 μm 光源泵浦，只能采用 2 μm、2.79 μm 等波段光源泵浦，这些波段的光源在输出能量或功率、光束质量及可靠性等方面相较于 1 μm 光源存在差距，进而限制了长波红外激光器的输出性能。未来，基于二阶非线性频率变换的长波红外激光器的发展方向主要在改良晶体缺陷性质、开发新型长波红外非线性晶体[99]、优化晶体大尺寸制备技术以及提升泵浦源性能等方面。此外，基于二阶非线性频率变换的长波红外激光器具有转换效率低的特点，随着 3～5 μm 中波红外光源的开发，长波红外激光器的性能将会得到进一步提升。

除了上述总结的二阶非线性频率变换技术外，基于三阶非线性效应的拉曼激光器也是实现波长由短波向长波转换的重要途径[100-101]。相较于二阶非线性频率变换，受激拉曼散射固有的自动相位匹配以及无空间烧孔效应的特点，使得拉曼激光器能够在晶体所覆盖的全透过光谱范围内实现高光束质量且窄光谱宽度的波长转换输出[102-106]。目前人们已经利用晶体拉曼实现了中红外波段的拉曼激光输出，而针对长波红外拉曼激光的研究却鲜有报道。近年来，金刚石晶体以其高拉曼增益系数（>10 cm·GW^{-1}@1 μm）、极宽的光谱透过范围（>0.23 μm 全波段）、已知晶体中最高的热导率（2000 W·m^{-1}·K^{-1}）和最大的拉曼频移（1332.3 cm^{-1}），成为拉曼激光技术研究领域的研究热点[107-112]。值得一提的是，金刚石晶体固有的大拉曼频

移使得金刚石拉曼激光器能够在3.8～4.7 μm波长激光的泵浦下，仅通过一阶拉曼转换便能够直接获得8～12 μm的长波红外激光输出，相关的理论研究结果已表明金刚石拉曼转换在获取长波红外激光上拥有巨大的潜力[112]。目前，实现长波红外金刚石拉曼高效率转换的难点在于获取满足金刚石拉曼增益线宽(1.5 cm^{-1})的大于3.8 μm的激光泵浦源，以及需要对拉曼振荡器参数进行优化，以克服波长变长导致的拉曼增益系数下降，这也是长波红外拉曼激光器未来实现高效率转换亟需攻克的难题。

参 考 文 献

[1] Bekman H H P T, van den Heuvel J C, van Putten F J M, et al. Development of a mid-infrared laser for study of infrared countermeasures techniques[J]. Proceedings of SPIE, 2004, 5615: 27-38.

[2] Sijan A. Development of military lasers for optical countermeasures in the mid-IR[J]. Proceedings of SPIE, 2009, 7483: 748304.

[3] Gabrieli A, Wright R, Lucey P G, et al. Characterization and initial field test of an 8-14 μm thermal infrared hyperspectral imager for measuring SO_2 in volcanic plumes[J]. Bulletin of Volcanology, 2016, 78(10): 73.

[4] Webber M E, Pushkarsky M B, Patel C K N. Optical detection of chemical warfare agents and toxic industrial chemicals: simulation[J]. Journal of Applied Physics, 2005, 97(11): 113101.

[5] Jha A. A review of visible, near-IR, and mid-IR transitions in rare-earth doped glass waveguides for remote sensing and LIDAR[J]. Proceedings of SPIE, 2006, 6409: 246-257.

[6] Quagliano J R, Stoutland P O, Petrin R R, et al. Quantitative chemical identification of four gases in remote infrared (9-11 μm) differential absorption lidar experiments[J]. Applied Optics, 1997, 36(9): 1915-1927.

[7] Serebryakov V A, Boĭko É V, Petrishchev N N, et al. Medical applications of mid-IR lasers. Problems and prospects[J]. Journal of Optical Technology, 2010, 77(1): 6-17.

[8] Serebryakov V S, Boĭko É V, Kalintsev A G, et al. Mid-IR laser for high-precision surgery[J]. Journal of Optical Technology, 2015, 82(12): 781-788.

[9] 王超臣, 刘瑞科, 王廷予, 等. 红外半导体激光器应用[J]. 激光杂志, 2020, 41(8): 1-10.
Wang C C, Liu R K, Wang T Y, et al. Applications of infrared semiconductor laser[J]. Laser Journal, 2020, 41(8): 1-10.

[10] Patel C K N. Continuous-wave laser action on vibrational-rotational transitions of CO_2[J]. Physical Review, 1964, 136(5A): A1187-A1193.

[11] Beaulieu A J. Transversely excited atmospheric pressure CO_2 lasers[J]. Applied Physics Letters, 1970, 16(12): 504-505.

[12] Youmans D G. Phase locking of adjacent channel leaky waveguide CO_2 lasers[J]. Applied Physics Letters, 1984, 44(4): 365-367.

[13] Allik T H, Chandra S, Rines D M, et al. Tunable 7-12 μm optical parametric oscillator using a Cr, Er: YSGG laser to pump CdSe and $ZnGeP_2$ crystals[J]. Optics Letters, 1997, 22(9): 597-599.

[14] Yang F, Yao J Y, Xu H Y, et al. Midinfrared optical parametric amplifier with 6.4-11 μm range based on $BaGa4Se_7$[J]. IEEE Photonics Technology Letters, 2015, 27(10): 1100-1103.

[15] Vitiello M S, Scalari G, Williams B, et al. Quantum cascade lasers: 20 years of challenges[J]. Optics Express, 2015, 23(4): 5167-5182.

[16] Faist J, Capasso F, Sivco D L, et al. Quantum cascade laser[J]. Science, 1994, 264(5158): 553-556.

[17] Faist J, Gmachl C, Capasso F, et al. Distributed feedback quantum cascade lasers[J]. Applied Physics Letters, 1997, 70(20): 2670-2672.

[18] Beck M, Hofstetter D, Aellen T, et al. Continuous wave operation of a mid-infrared semiconductor laser at room temperature[J]. Science, 2002, 295(5553): 301-305.

[19] Troccoli M, Lyakh A, Fan J, et al. Long-wave IR quantum cascade lasers for emission in the $\lambda=8$-12 μm spectral region[J]. Optical Materials Express, 2013, 3(9): 1546-1560.

[20] 邓凯, 高志远, 韩隆, 等. 量子级联激光器及其应用的研究进展[J]. 光电技术应用, 2021, 36(5): 23-29, 35.
Deng K, Gao Z Y, Han L, et al. Applications and progress of quantum cascade lasers[J]. Electro-Optic Technology Application, 2021, 36(5): 23-29, 35.

[21] 刘峰奇, 张锦川, 刘俊岐, 等. 量子级联激光器研究进展[J]. 中国激光, 2020, 47(7): 0701007.
Liu F Q, Zhang J C, Liu J Q, et al. Progress in quantum cascade lasers[J]. Chinese Journal of Lasers, 2020, 47(7): 0701007.

[22] Herbst R L, Byer R L. Singly resonant CdSe infrared parametric oscillator[J]. Applied Physics Letters, 1972, 21(5): 189-191.

[23] Oudar J L, Kupecek P J, Chemla D S. Medium infrared tunable down conversion of a YAG-pumped infrared dye laser in gallium selenide[J]. Optics Communications, 1979, 29(1): 119-122.

[24] Ketteridge P, Budni P, Lee I, et al. 8 micron ZGP OPO pumped at 2 microns[C]//Advanced Solid State Lasers, January 31, 1996, San Francisco, California. Washington, D.C.: Optica Publishing Group, 1996: OP8.

[25] Levi O, Pinguet T J, Skauli T, et al. Difference frequency generation of 8-μm radiation in orientation-patterned GaAs[J]. Optics Letters, 2002, 27(23): 2091-2093.

[26] Maidment L, Schunemann P G, Reid D T. Molecular fingerprint-region spectroscopy from 5 to 12 μm using an orientation-patterned gallium phosphide optical parametric oscillator[J]. Optics Letters, 2016, 41(18): 4261-4264.

[27] Kostyukova N Y, Boyko A A, Badikov V, et al. Widely tunable in the mid-IR $BaGa_4Se_7$ optical parametric oscillator pumped at 1064 nm[J]. Optics Letters, 2016, 41(15): 3667-3670.

[28] 彭雅珮, 姜本学, 范金太, 等. 激光二极管直接抽运中红外固体激光材料综述[J]. 激光与光电子学进展, 2015, 52(2): 020001.
Peng Y P, Jiang B X, Fan J T, et al. Review of mid-infrared laser materials directly pumped by laser-diode[J]. Laser & Optoelectronics Progress, 2015, 52(2): 020001.

[29] 徐飞, 潘其坤, 陈飞, 等. 中红外 Fe^{2+}: ZnSe激光器研究进展[J]. 中国光学, 2021, 14(3): 458-469.
Xu F, Pan Q K, Chen F, et al. Development progress of Fe^{2+}: ZnSe lasers[J]. Chinese Optics, 2021, 14(3): 458-469.

[30] 陈毅, 刘高佑, 王瑞雪, 等. 非线性晶体应用于中长波红外固体激光器的研究进展[J]. 人工晶体学报, 2020, 49(8): 1379-1395.
Chen Y, Liu G Y, Wang R X, et al. Research progress of nonlinear crystal applied in mid-and long-wave infrared solid-state laser[J]. Journal of Synthetic Crystals, 2020, 49(8): 1379-1395.

[31] Yao J Y, Mei D J, Bai L, et al. $BaGa_4Se_7$: a new congruent-melting IR nonlinear optical material[J]. Inorganic Chemistry, 2010, 49(20): 9212-9216.

[32] Peterson R D, Whelan D, Bliss D, et al. Improved material quality and OPO performance in orientation-patterned GaAs[J]. Proceedings of SPIE, 2009, 7197: 719709.

[33] 王健, 程红娟, 高彦昭. 长波红外用准相位匹配材料研究进展[J]. 人工晶体学报, 2020, 49(8): 1397-1404, 1442.
Wang J, Cheng H J, Gao Y Z. Research progress of quasi-phase matching materials for long-wave IR generation[J]. Journal of

Synthetic Crystals, 2020, 49(8): 1397-1404, 1442.
[34] Vodopyanov K L, Voevodin V G. Type I and Ⅱ $ZnGeP_2$ travelling-wave optical parametric generator tunable between 3.9 and 10 μm[J]. Optics Communications, 1995, 117(3/4): 277-282.
[35] Zawilski K T, Schunemann P G, Setzler S D, et al. Large aperture single crystal $ZnGeP_2$ for high-energy applications[J]. Journal of Crystal Growth, 2008, 310(7/8/9): 1891-1896.
[36] Zelmon D E, Hanning E A, Schunemann P G. Refractive-index measurements and Sellmeier coefficients for zinc germanium phosphide from 2 to 9 μm with implications for phase matching in optical frequency-conversion devices[J]. Journal of the Optical Society of America B, 2001, 18(9): 1307-1310.
[37] Yelisseyev A P, Lobanov S I, Krinitsin P G, et al. The optical properties of the nonlinear crystal $BaGa_4Se_7$[J]. Optical Materials, 2020, 99: 109564.
[38] Yao J Y, Yin W L, Feng K, et al. Growth and characterization of $BaGa_4Se_7$ crystal[J]. Journal of Crystal Growth, 2012, 346(1): 1-4.
[39] Ni Y B, Wu H X, Mao M S, et al. Growth and characterization of mid-far infrared optical material CdSe crystal[J]. Optical Materials Express, 2018, 8(7): 1796-1805.
[40] Yao B Q, Li G, Zhu G L, et al. Comparative investigation of long-wave infrared generation based on $ZnGeP_2$ and CdSe optical parametric oscillators[J]. Chinese Physics B, 2012, 21(3): 034213.
[41] Beasley J D. Thermal conductivities of some novel nonlinear optical materials[J]. Applied Optics, 1994, 33(6): 1000-1003.
[42] Finsterbusch K, Bayer A, TunableZacharias H. Tunable, narrow-band picosecond radiation in the mid-infrared by difference frequency mixing in GaSe and CdSe[J]. Applied Physics B, 2004, 79(4): 457-462.
[43] Zhang H Z, Kang Z H, Jiang Y, et al. SHG phase matching in GaSe and mixed $GaSe_{1-x}S_x$, $x\leqslant 0.412$, crystals at room temperature[J]. Optics Express, 2008, 16(13): 9951-9957.
[44] Chen C W, Hsu Y K, Huang J Y, et al. Generation properties of coherent infrared radiation in the optical absorption region of GaSe crystal[J]. Optics Express, 2006, 14(22): 10636-10644.
[45] Isaenko L I, Yelisseyev A P. Recent studies of nonlinear chalcogenide crystals for the mid-IR[J]. Semiconductor Science and Technology, 2016, 31(12): 123001.
[46] Kieleck C, Hildenbrand A, Eichhorn M, et al. OP-GaAs OPO pumped by 2 μm *Q*-switched lasers: Tm; Ho∶silica fiber laser and Ho∶YAG laser[J]. Proceedings of SPIE, 2010, 7836: 783607.
[47] Schunemann P G, Zawilski K T, Pomeranz L A, et al. Advances in nonlinear optical crystals for mid-infrared coherent sources[J]. Journal of the Optical Society of America B, 2016, 33(11): D36-D43.
[48] Schunemann P G, Pomeranz L A, Magarrell D J. First OPO based on orientation-patterned gallium phosphide (OP-GaP)[C]//CLEO: Science and Innovations 2015, May 10-15, 2015, San Jose, California, USA. Washington, D.C.: Optica Publishing Group, 2015: SW3O.1.
[49] Devi K, Padhye A, Schunemann P G, et al. Multimilliwatt, tunable, continuous-wave, mid-infrared generation across 4.6-4.7 μm based on orientation-patterned gallium phosphide[J]. Optics Letters, 2018, 43(10): 2284-2287.
[50] Bakkland A, Fonnum H, Lippert E, et al. Long-wave infrared source with 45 mJ pulse energy based on nonlinear conversion in $ZnGeP_2$[C]//CLEO: Science and Innovations 2016, June 5-10, 2016, San Jose, California, USA. Washington, D.C.: Optica Publishing Group, 2016: STu1Q.8.
[51] Yu K K, Liang Z Q, Yan X S. Experimental studies on beam quality-improving of 8 μm ZGP optical parametric oscillator[C]//2015 International Conference on Optoelectronics and Microelectronics (ICOM), July 16-18, 2015, Changchun, China. New York: IEEE Press, 2015: 34-37.
[52] Qian C P, Shen Y J, Dai T Y, et al. High power far-infrared optical parametric oscillator with high beam quality[J]. Proceedings of SPIE, 2016, 10016: 100160G.
[53] Qian C P, Shen Y J, Yao B Q, et al. High power far-infrared ZGP OPO laser[C]//Conference on Lasers and Electro-Optics 2016, June 5-10, 2016, San Jose, California, USA. Washington, D.C.: Optica Publishing Group, 2016: ATh3J.6.
[54] Li L J, Yang X N, Yang Y Q, et al. A high-power, long-wavelength infrared $ZnGeP_2$ OPO pumped by a *Q*-switched Tm, Ho: $GdVO_4$ laser[J]. Journal of Russian Laser Research, 2017, 38(3): 305-310.
[55] Qian C P, Duan X M, Yao B Q, et al. 11.4 W long-wave infrared source based on $ZnGeP_2$ optical parametric amplifier[J]. Optics Express, 2018, 26(23): 30195-30201.
[56] Liu G Y, Chen Y, Yao B Q, et al. Study on long-wave infrared $ZnGeP_2$ subsequent optical parametric amplifiers with different types of phase matching of $ZnGeP_2$ crystals[J]. Applied Physics B, 2019, 125(12): 233.
[57] Liu G Y, Chen Y, Yao B Q, et al. 3.5 W long-wave infrared $ZnGeP_2$ optical parametric oscillator at 9.8 μm[J]. Optics Letters, 2020, 45(8): 2347-2350.
[58] 魏磊, 吴德成, 刘东, 等. Ho∶YLF 激光泵浦的长波红外 $ZnGeP_2$ 光参量振荡器[J]. 中国激光, 2021, 48(1): 0101002.
Wei L, Wu D C, Liu D, et al. Long-wave infrared $ZnGeP_2$ optical parametric oscillator pumped by Ho∶YLF laser[J]. Chinese Journal of Lasers, 2021, 48(1): 0101002.
[59] Qian C P, Yu T, Liu J, et al. A high-energy, narrow-pulse-width, long-wave infrared laser based on ZGP crystal[J]. Crystals, 2021, 11(6): 656.
[60] Qian C P, Yu T, Liu J, et al. 5.4 W, 9.4 ns pulse width, long-wave infrared ZGP OPO pumped by Ho∶YAG MOPA system [J]. IEEE Photonics Journal, 2021, 13(3): 1501008.
[61] Zhao B R, Chen Y, Yao B Q, et al. High-efficiency, tunable 8-9 μm $BaGa_4Se_7$ optical parametric oscillator pumped at 2.1 μm [J]. Optical Materials Express, 2018, 8(11): 3332-3337.
[62] Kolker D B, Sherstov I V, Kostyukova N Y, et al. Broadband tunable source of mid-IR laser radiation for photoacoustic spectroscopy[J]. Quantum Electronics, 2019, 49(1): 29-34.
[63] Hu S W, Wang L, Guo Y W, et al. High-conversion-efficiency tunable mid-infrared $BaGa_4Se_7$ optical parametric oscillator pumped by a 2.79-μm laser[J]. Optics Letters, 2019, 44(9): 2201-2203.
[64] Yang F, Yao J Y, Guo Y W, et al. High-energy continuously tunable 8-14 μm picosecond coherent radiation generation from BGSe-OPA pumped by 1064 nm laser[J]. Optics & Laser Technology, 2020, 125: 106040.
[65] Xu D G, Zhang J X, He Y X, et al. High-energy, tunable long-wave mid-infrared optical parametric oscillator based on $BaGa_4Se_7$ crystal[J]. Optics Letters, 2020, 45(18): 5287-5290.
[66] Zhang J W, Wang Q, Hao J J, et al. Broadband, few-cycle mid-infrared continuum based on the intra-pulse difference frequency generation with BGSe crystals[J]. Optics Express, 2020, 28(25): 37903-37909.
[67] Yuan J H, Duan X M, Yao B Q, et al. Tunable 10- to 11-μm CdSe optical parametric oscillator pumped by a 2.1-μm Ho∶YAG laser[J]. Applied Physics B, 2016, 122(7): 202.
[68] Yuan J H, Chen Y, Duan X M, et al. CdSe optical parametric oscillator operating at 12.07 μm with 170 mW output[J]. Optics & Laser Technology, 2017, 92: 1-4.
[69] Wang J, Yuan L G, Zhang Y W, et al. Generation of 320 mW at 10.20 μm based on CdSe long-wave infrared crystal[J]. Journal of Crystal Growth, 2018, 491: 16-19.
[70] Chen Y, Liu G Y, Yang C, et al. 1 W, 10.1 μm, CdSe optical parametric oscillator with continuous-wave seed injection[J]. Optics Letters, 2020, 45(7): 2119-2122.
[71] Chen Y, Yang C, Liu G Y, et al. 11 μm, high beam quality

idler-resonant CdSe optical parametric oscillator with continuous-wave injection-seeded at 2.58 μm[J]. Optics Express, 2020, 28(11): 17056-17063.

[72] Yang K, Li J H, Gao Y Z, et al. Watt-level long-wave infrared CdSe pulsed-nanosecond optical parametric oscillator[J]. Optics & Laser Technology, 2022, 145: 107491.

[73] 魏磊, 李宝, 陈国, 等. 长波红外CdSe光参量振荡器[J]. 中国激光, 2021, 48(24): 2401004.
Wei L, Li B, Chen G, et al. Long-wave infrared CdSe optical parametric oscillator[J]. Chinese Journal of Lasers, 2021, 48(24): 2401004.

[74] Gaida C, Gebhardt M, Heuermann T, et al. Watt-scale super-octave mid-infrared intrapulse difference frequency generation[J]. Light: Science & Applications, 2018, 7: 94.

[75] Yan D X, Xu D G, Wang Y Y, et al. High-repetition-rate, tunable and coherent mid-infrared source based on difference frequency generation from a dual-wavelength 2 μ m laser and GaSe crystal[J]. Laser Physics, 2018, 28(12): 126205.

[76] Liu K, Liang H K, Li W K, et al. Microjoule sub-two-cycle mid-infrared intrapulse-DFG driven by 3 μm OPCPA[J]. IEEE Photonics Technology Letters, 2019, 31(21): 1741-1744.

[77] Liu K, Liang H K, Wang L F, et al. Multi-microjoule GaSe-based midinfrared optical parametric amplifier with an ultrabroad idler spectrum covering 4.2-16 μm[J]. Optics Letters, 2019, 44(4): 1003-1006.

[78] Butler T P, Gerz D, Hofer C, et al. Watt-scale 50-MHz source of single-cycle waveform-stable pulses in the molecular fingerprint region[J]. Optics Letters, 2019, 44(7): 1730-1733.

[79] Yoshioka K, Igarashi I, Yoshida S, et al. Subcycle mid-infrared coherent transients at 4 MHz repetition rate applicable to light-wave-driven scanning tunneling microscopy[J]. Optics Letters, 2019, 44(21): 5350-5353.

[80] 姚宝权, 杨科, 密淑一, 等. 高功率Ho∶YAG激光器及其泵浦的磷锗锌、硒镓钡和硒化镉中长波红外非线性光学频率转换研究进展[J]. 中国激光, 2022, 49(1): 0101002.
Yao B Q, Yang K, Mi S Y, et al. Research progress of high-power Ho∶YAG lasers and its application for pumping mid-far-infrared nonlinear frequency conversion in ZGP, BGSe and CdSe crystals[J]. Chinese Journal of Lasers, 2022, 49(1): 0101002.

[81] 温雅, 吴春婷, 袁泽锐, 等. 远红外固体激光器研究进展[J]. 中国光学, 2018, 11(6): 889-900.
Wen Y, Wu C T, Yuan Z R, et al. Research progress of far-infrared solid-state lasers[J]. Chinese Optics, 2018, 11(6): 889-900.

[82] Chen B H, Nagy T, Baum P. Efficient middle-infrared generation in $LiGaS_2$ by simultaneous spectral broadening and difference-frequency generation[J]. Optics Letters, 2018, 43(8): 1742-1745.

[83] Isaenko L, Yelisseyev A, Lobanov S, et al. Growth and properties of $LiGaX_2$ (X=S, Se, Te) single crystals for nonlinear optical applications in the mid-IR[J]. Crystal Research and Technology, 2003, 38(35): 379-387.

[84] Petrov V. Frequency down-conversion of solid-state laser sources to the mid-infrared spectral range using non-oxide nonlinear crystals[J]. Progress in Quantum Electronics, 2015, 42: 1-106.

[85] Pupeza I, Sánchez D, Zhang J, et al. High-power sub-two-cycle mid-infrared pulses at 100 MHz repetition rate[J]. Nature Photonics, 2015, 9(11): 721-724.

[86] Morimoto T, Sono N, Miyamoto T, et al. Generation of a carrier-envelope-phase-stable femtosecond pulse at 10 μm by direct down-conversion from a Ti∶sapphire laser pulse[J]. Applied Physics Express, 2017, 10(12): 122701.

[87] Chen B H, Wittmann E, Morimoto Y, et al. Octave-spanning single-cycle middle-infrared generation through optical parametric amplification in $LiGaS_2$[J]. Optics Express, 2019, 27(15): 21306-21318.

[88] Heiner Z, Wang L, Petrov V, et al. Broadband vibrational sum-frequency generation spectrometer at 100 kHz in the 950-1750 cm^{-1} spectral range utilizing a $LiGaS_2$ optical parametric amplifier[J]. Optics Express, 2019, 27(11): 15289-15297.

[89] Qu S Z, Liang H K, Liu K, et al. 9 μm few-cycle optical parametric chirped-pulse amplifier based on $LiGaS_2$[J]. Optics Letters, 2019, 44(10): 2422-2425.

[90] Schunemann P G, Pomeranz L A, Setzler S D, et al. CW mid-IR OPO based on OP-GaAs[C]//2013 Conference on Lasers & Electro-Optics Europe & International Quantum Electronics Conference CLEO EUROPE/IQEC, May 12-16, 2013, Munich, Germany. New York: IEEE Press, 2013.

[91] Vodopyanov K L, Makasyuk I, Schunemann P G. Grating tunable 4-14 μm GaAs optical parametric oscillator pumped at 3 μm[J]. Optics Express, 2014, 22(4): 4131-4136.

[92] Clément Q, Melkonian J M, Dherbecourt J B, et al. Longwave infrared, single-frequency, tunable, pulsed optical parametric oscillator based on orientation-patterned GaAs for gas sensing[J]. Optics Letters, 2015, 40(12): 2676-2679.

[93] Wueppen J, Nyga S, Jungbluth B, et al. 1.95 μm-pumped OP-GaAs optical parametric oscillator with 10.6 μm idler wavelength [J]. Optics Letters, 2016, 41(18): 4225-4228.

[94] Gutty F, Grisard A, Larat C, et al. 140 W peak power laser system tunable in the LWIR[J]. Optics Express, 2017, 25(16): 18897-18906.

[95] Boyko A A, Schunemann P G, Guha S, et al. Optical parametric oscillator pumped at ~1 μm with intracavity mid-IR difference-frequency generation in OP-GaAs[J]. Optical Materials Express, 2018, 8(3): 549-554.

[96] Wang L, Chen W D, Schunemann P, et al. Nanosecond optical parametric oscillator with midinfrared intracavity difference-frequency mixing in orientation-patterned GaAs[J]. Optics Letters, 2021, 46(2): 332-335.

[97] Maidment L, Kara O, Schunemann P G, et al. Long-wave infrared generation from femtosecond and picosecond optical parametric oscillators based on orientation-patterned gallium phosphide[J]. Applied Physics B, 2018, 124(7): 143.

[98] Schunemann P G, Johnson K, Farrell C, et al. Continuous wavelength tuning from 3.9-12 μm from an optical parametric oscillator based on orientation-patterned GaP grown on GaAs[J]. Optical Materials Express, 2021, 11(3): 654-663.

[99] 王振友, 吴海信. 8～12 μm长波红外非线性晶体研究进展[J]. 人工晶体学报, 2019, 48(1): 34-46, 53.
Wang Z Y, Wu H X. Research progress of nonlinear crystals for 8-12 μm long-wave IR generation[J]. Journal of Synthetic Crystals, 2019, 48(1): 34-46, 53.

[100] Piper J A, Pask H M. Crystalline Raman lasers[J]. IEEE Journal of Selected Topics in Quantum Electronics, 2007, 13(3): 692-704.

[101] Williams R J, Kitzler O, Bai Z X, et al. High power diamond Raman lasers[J]. IEEE Journal of Selected Topics in Quantum Electronics, 2018, 24(5): 1602214.

[102] McKay A, Kitzler O, Mildren R P. Simultaneous brightness enhancement and wavelength conversion to the eye-safe region in a high-power diamond Raman laser[J]. Laser & Photonics Reviews, 2014, 8(3): L37-L41.

[103] Bai Z X, Williams R J, Kitzler O, et al. 302 W quasi-continuous cascaded diamond Raman laser at 1.5 microns with large brightness enhancement[J]. Optics Express, 2018, 26(16): 19797-19803.

[104] Bai Z X, Williams R J, Jasbeer H, et al. Large brightness enhancement for quasi-continuous beams by diamond Raman laser conversion[J]. Optics Letters, 2018, 43(3): 563-566.

[105] Lux O, Sarang S, Kitzler O, et al. Intrinsically stable high-power single longitudinal mode laser using spatial hole burning free gain[J]. Optica, 2016, 3(8): 876-881.

[106] 白振旭, 陈晖, 李宇琪, 等. 基于金刚石拉曼转换的光束亮度增强研究进展[J]. 红外与激光工程, 2021, 50(1): 20200098.
Bai Z X, Chen H, Li Y Q, et al. Development of beam brightness enhancement based on diamond Raman conversion[J]. Infrared and Laser Engineering, 2021, 50(1): 20200098.
[107] Mildren R P, Rabeau J R. Optical engineering of diamond[M]. Singapore: John Wiley & Sons Inc, 2013.
[108] Williams R J, Nold J, Strecker M, et al. Efficient Raman frequency conversion of high-power fiber lasers in diamond[J]. Laser & Photonics Reviews, 2015, 9(4): 405-411.
[109] Antipov S, Sabella A, Williams R J, et al. 1.2 kW quasi-steady-state diamond Raman laser pumped by an M^2=15 beam[J]. Optics Letters, 2019, 44(10): 2506-2509.
[110] 白振旭, 杨学宗, 陈晖, 等. 高功率金刚石激光技术研究进展[J]. 红外与激光工程, 2020, 49(12): 20201076.
Bai Z X, Yang X Z, Chen H, et al. Research progress of high-power diamond laser technology[J]. Infrared and Laser Engineering, 2020, 49(12): 20201076.
[111] 白振旭, 陈晖, 丁洁, 等. 基于空间光腔的高功率布里渊频率梳[J]. 中国激光, 2022, 49(4): 0415001.
Bai Z X, Chen H, Ding J, et al. High-power Brillouin frequency comb based on free-space optical cavity[J]. Chinese Journal of Lasers, 2022, 49(4): 0415001.
[112] Chen H, Bai Z X, Zhao C, et al. Numerical simulation of long-wave infrared generation using an external cavity diamond Raman laser[J]. Frontiers in Physics, 2021, 9: 671559.

Research Progress of Long-Wave Infrared Lasers Based on Nonlinear Frequency Conversion

Bai Zhenxu[1,2*], Gao Jia[1,2], Zhao Chen[1,2,3], Yan Bingzheng[1,2], Qi Yaoyao[1,2], Ding Jie[1,2], Wang Yulei[1,2], Lü Zhiwei[1,2**]

[1]*Center for Advanced Laser Technology, Hebei University of Technology, Tianjin* 300401, *China*;
[2]*Hebei Key Laboratory of Advanced Laser Technology and Equipment, Tianjin* 300401, *China*;
[3]*Science and Technology on Electro-Optical Information Security Control Laboratory, Tianjin* 300308, *China*

Abstract

Significance The 8-12 μm long-wave infrared (LWIR) laser, which is within the atmospheric transmission window and the eye-safe range and demonstrates a higher transmittance in atmospheric media (Fig. 1), has critical applications in various fields, such as directed infrared countermeasures, environmental monitoring, lidar, and surgery. For example, the laser in this LWIR band plays an important role in environmental monitoring and differential absorption lidar because this band covers the fundamental absorption bands of many gas molecules, such as H_2O, CO_2, NH3, and O_3. In terms of medical treatment, the 8-12 μm LWIR laser, with a large absorption coefficient and a shallow penetration depth in water and other components of biological tissues, serves as a unique and effective tool in biological tissue treatment. In addition, high-energy 8-12 μm LWIR lasers are in high demand in the field of defense.

At present, approaches to 8-12 μm LWIR laser mainly include direct radiation from gain media represented by carbon dioxide (CO_2) lasers and semiconductor quantum cascade lasers (QCLs) and nonlinear optical techniques represented by second-order nonlinear frequency conversion. CO_2 lasers have been one of the most mature coherent radiation sources for the LWIR band since the invention of the first CO_2 laser in 1964. However, their output wavelengths are limited to the spectral lines of 9.2-9.8 μm and 10.1-11 μm. In addition, since CO_2 lasers usually need to be supported by a large cooling system, the overall size of the device is huge, which greatly limits the application range of CO_2 lasers. QCLs feature a broad emission spectrum (3.5-160 μm) with a relatively narrow linewidth and favorable wavelength tunability. However, due to the limited depth of their quantum wells, QCLs offer low efficiency in the 8-12 μm band and consequently fail to achieve high-power and high-pulse energy operation. Besides, they are difficult to design and entail a relatively high manufacturing cost.

Although 8-12 μm LWIR lasing has already been achieved with gas and semiconductor as gain media, no mature method of LWIR lasing by directly pumping crystalline gain media is obtained so far due to the restriction of the intrinsic emission spectra of the currently available crystals. As the most mature and most widely used method, nonlinear frequency conversion is an effective approach to 8-12 μm lasing. Notably, solid-state lasers based on second-order nonlinear frequency conversion techniques break through the predicament that crystalline gain media cannot directly achieve LWIR lasing. Furthermore, compared with CO_2 lasers and QCLs, all-solid-state lasers based on nonlinear frequency conversion techniques have the characteristics of excellent wavelength tunability and power scalability. The diversities of the available pump parameters (wavelength, width, energy, power, etc.) and emerging nonlinear optical crystals provide LWIR lasers based on nonlinear frequency conversion with a broader development space towards but not limited to ultrashort pulse width, high repetition rate, wide wavelength tuning range, high energy, and high power. This paper reviews the working

mechanisms and research progress of LWIR lasers based on second-order nonlinear frequency conversion to provide a reference for the personnel engaged in the research and development of lasers.

Progress Specifically, the working principles and characteristics of the second-order nonlinear frequency conversion techniques, including optical parametric generation (OPG), optical parametric oscillation (OPO), difference frequency generation (DFG), and optical parametric amplification (OPA), are described (Fig. 3). Subsequently, the physical and nonlinear optical properties, including nonlinear coefficient, transparency range, thermal conductivity, and damage threshold, of commonly used nonlinear crystals, such as $ZnGeP_2$, $BaGa4Se_7$, CdSe, GaSe, $LiGaS_2$, orientation-patterned GaAs, and orientation-patterned GaP, are summarized (Table 1). Then, the detailed properties of different crystals and the output characteristics of the corresponding LWIR laser based on the crystals are analyzed. The research progress analysis shows that LWIR lasers based on second-order nonlinear frequency conversion have achieved femtosecond, picosecond, and nanosecond output in pulse width and repetition rates ranging from several hertz to megahertz. However, due to the low inherent quantum conversion efficiency of nonlinear frequency conversion towards the LWIR band (pumped by 1-3 μm near- and mid-infrared lasers), the output energy of the LWIR lasers is mainly at the microjoule and millijoule levels at present (Fig. 10). Finally, the opportunities and challenges for LWIR lasers based on second-order frequency conversion techniques are discussed, and the potential method of LWIR lasing via Raman conversion based on the third-order nonlinear effect and its prospect are presented.

Conclusions and Prospects Crystalline LWIR lasers based on second-order nonlinear frequency conversion techniques have made outstanding achievements in ultrashort pulse width, high repetition rate, wide wavelength tuning range, and high peak power. The improvement of crystal growth technique, the emergence of new types of nonlinear optical crystals, and the development of currently available crystals with higher optical quality and larger volume crystals pave the way for the further improvement of the power and conversion efficiencies of LWIR lasers. In addition to the above reviewed second-order nonlinear frequency conversion techniques, diamond Raman lasers (based on the third-order nonlinear optical effect) with an extremely wide spectral transmission range and an extremely high thermal conductivity are considered a promising way of wavelength conversion from short-wave to long-wave.

Key words lasers; long-wave infrared laser; nonlinear frequency conversion; 8-12 μm; nonlinear crystal